Small-molecule MAPK inhibitors restore radioiodine incorporation in mouse thyroid cancers with conditional BRAF activation

Debyani Chakravarty,[1] Elmer Santos,[2] Mabel Ryder,[1,3] Jeffrey A. Knauf,[1] Xiao-Hui Liao,[4] Brian L. West,[5] Gideon Bollag,[5] Richard Kolesnick,[3,6] Tin Htwe Thin,[6] Neal Rosen,[3,6] Pat Zanzonico,[2,7] Steven M. Larson,[2,6] Samuel Refetoff,[4,8,9] Ronald Ghossein,[10] and James A. Fagin[1,3]

[1]Human Oncology and Pathogenesis Program, [2]Department of Radiology, and [3]Department of Medicine, Memorial Sloan-Kettering Cancer Center, New York, New York, USA. [4]Department of Medicine, University of Chicago, Chicago, Illinois, USA. [5]Plexxikon Inc., Berkeley, California, USA. [6]Department of Molecular Pharmacology and Chemistry and [7]Department of Medical Physics, Memorial Sloan-Kettering Cancer Center, New York, New York, USA. [8]Department of Pediatrics and [9]Committee on Genetics, University of Chicago, Chicago, Illinois, USA. [10]Department of Pathology, Memorial Sloan-Kettering Cancer Center, New York, New York, USA.

Advanced human thyroid cancers, particularly those that are refractory to treatment with radioiodine (RAI), have a high prevalence of BRAF (v-raf murine sarcoma viral oncogene homolog B1) mutations. However, the degree to which these cancers are dependent on BRAF expression is still unclear. To address this question, we generated mice expressing one of the most commonly detected BRAF mutations in human papillary thyroid carcinomas ($BRAF^{V600E}$) in thyroid follicular cells in a doxycycline-inducible (dox-inducible) manner. Upon dox induction of $BRAF^{V600E}$, the mice developed highly penetrant and poorly differentiated thyroid tumors. Discontinuation of dox extinguished $BRAF^{V600E}$ expression and reestablished thyroid follicular architecture and normal thyroid histology. Switching on $BRAF^{V600E}$ rapidly induced hypothyroidism and virtually abolished thyroid-specific gene expression and RAI incorporation, all of which were restored to near basal levels upon discontinuation of dox. Treatment of mice with these cancers with small molecule inhibitors of either MEK or mutant BRAF reduced their proliferative index and partially restored thyroid-specific gene expression. Strikingly, treatment with the MAPK pathway inhibitors rendered the tumor cells susceptible to a therapeutic dose of RAI. Our data show that thyroid tumors carrying $BRAF^{V600E}$ mutations are exquisitely dependent on the oncoprotein for viability and that genetic or pharmacological inhibition of its expression or activity is associated with tumor regression and restoration of RAI uptake in vivo in mice. These findings have potentially significant clinical ramifications.

Introduction

The gain-of-function $BRAF^{T1799A}$ mutation accounts for 70% of melanomas (1) and 40% of thyroid cancers (2). In the latter, *BRAF* mutations are associated with poor prognosis (3–5), and are overrepresented in advanced [^{18}F]-fluorodeoxyglucose–PET–positive metastatic thyroid tumors (6). Conventional treatment, including adjuvant therapy with ^{131}I-iodide, is of marginal benefit for these cancers, as they no longer have the ability to trap iodide efficiently.

BRAF mutations are found in approximately 25% of micropapillary carcinomas, which has been taken as evidence that activation of this oncogene may be a tumor-initiating event (3–7). Oncoproteins involved in tumor initiation are often drivers of the disease. The concept of "oncogene addiction" refers to the reprogramming of tumor cells by which a driver oncoprotein hijacks the control of cell growth, such that the cancer cells become dependent on its continued activity for their viability (8). Although oncogene addiction has been extensively studied in vitro (9–15), arguably the most persuasive evidence for its significance has come from mouse models with conditional oncogene activation. In the first in vivo example, doxycycline (dox) activation of MYC (v-myc myelocytomatosis viral related oncogene) in hematopoietic cells resulted in T cell and myeloid leukemias, and its deinduction was followed by apoptosis and/or cellular senescence (16). A number of other tetracycline-inducible mouse models have supported this initial observation in different lineages and with a variety of oncoproteins, i.e., *Hras* in melanoma (17), *Kras* in lung adenocarcinoma (18), *Bcr-Abl* in B cell lymphoma/leukemia (19), and *Erbb2* in breast cancer (20). Conditional activation of a latent endogenous *Braf* allele in mouse melanocytes results in hyperpigmentation and development of nevi that have features consistent with oncogene-induced senescence, which after a longer latency, progress to amelanotic malignant melanomas that do not spontaneously metastasize (21).

Here we describe the development of transgenic mice with dox-inducible expression of $BRAF^{V600E}$ in thyroid follicular cells. Upon dox administration, murine thyroid tumors induced by $BRAF^{V600E}$ phenotypically resembled high-grade papillary thyroid cancers (PTC) found in humans, which were exquisitely dependent upon the presence of the oncoprotein for viability. The canonical signaling pathway triggered by BRAF is thought to result in the near-exclusive activation of MEK and ERK. Thus, BRAF-positive thyroid cancer cell lines are sensitive to the growth-suppressive effects of MAPK pathway inhibitors (22–25), consistent with findings in other lineages (26, 27). We therefore determined whether selective antagonists of mutant BRAF (PLX4720) or MEK (PD0325901)

Conflict of interest: Brian L. West and Gideon Bollag are employees of Plexxikon Inc. Neal Rosen received honoraria from Roche Pharmaceuticals.

Citation for this article: *J Clin Invest.* 2011;121(12):4700–4711. doi:10.1172/JCI46382.

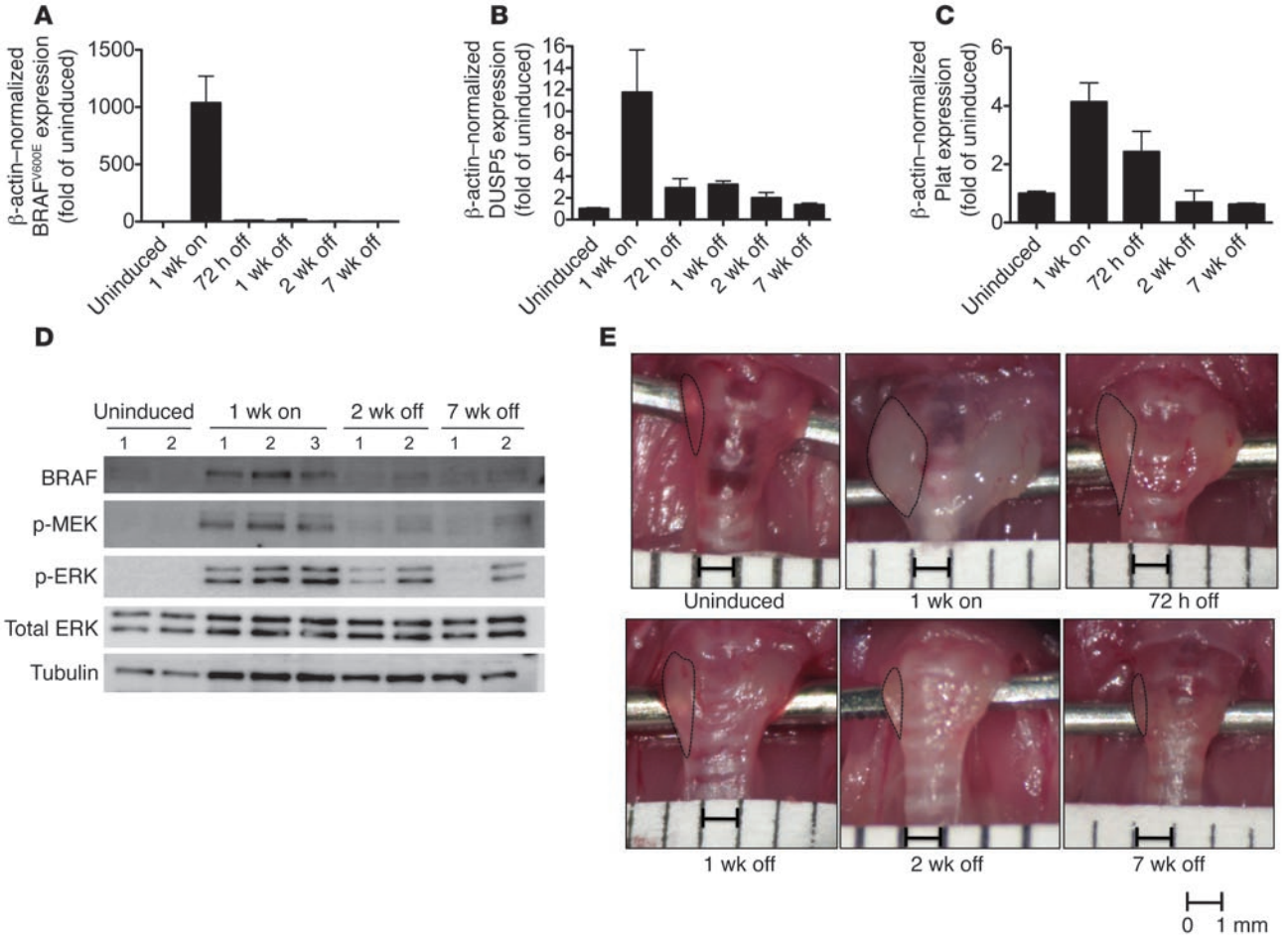

Figure 1

Inducible *BRAF^{V600E}* expression in thyroid cells reversibly activates MAPK signaling and thyroid growth. Eight-week-old *Tg-rtTA/tetO-BRAF^{V600E}* mice were fed dox-chow (on) for 1 week and then regular chow (off) for the indicated times. (**A**–**C**) qRT-PCR was performed to measure gene expression levels of mutant BRAF (**A**), DUSP5 (**B**), or PLAT (**C**) after normalization to β-actin. Bars represent mean ± SEM ($n \geq 8$ animals/group). (**D**) Western blots of protein lysates from thyroid tissue probed with antibodies to BRAF, p-MEK, p-ERK1/2, total ERK1/2, or tubulin. (**E**) Representative gross appearance of thyroid glands of *Tg-rtTA/tetO-BRAF^{V600E}* at the indicated times. The boundaries of the thyroid are demarcated by dashed lines. Scale bar: 1 mm.

phenocopied the dramatic regression of these tumors and the effects on thyroid function that occurred after genetic withdrawal of BRAF^{V600E}. Our findings are consistent with a reversal of some, but not all, of the properties of BRAF-induced PTC by these agents. Most prominent was the clear restoration of iodine incorporation in these tumors, which rendered them susceptible to therapeutic doses of radioiodine (RAI), an approach that could be used to advantage as a therapeutic strategy for this disease.

Results

Inducible expression of oncogenic BRAF in thyroid cells reversibly activates MAPK signaling. To express inducible human oncogenic BRAF in mouse thyroid follicular cells, we generated *Tg-rtTA/tetO-BRAF^{V600E}* mice (Supplemental Figure 1; supplemental material available online with this article; doi:10.1172/JCI46382DS1). Expression of *BRAF^{V600E}* mRNA was already induced by 24 hours (not shown), continuously sustained in the presence of dox, and switched off when dox was withdrawn (Figure 1A). Accordingly, total BRAF protein, p-MEK, and p-ERK levels were induced by dox and reversed by its withdrawal (Figure 1C). Expression of DUSP-5 and PLAT, which are measures of MAPK transcriptional output, was induced 10- and 4-fold, respectively, 1 week after dox treatment, returning to near-basal levels after dox removal (Figure 1, B and C).

Induction of oncogenic BRAF in Tg-rtTA/tetO-BRAF^{V600E} mice results in papillary thyroid cancers with poorly differentiated features. None of the *Tg-rtTA/tetO-BRAF^{V600E}* mice developed thyroid abnormalities through at least 18 weeks in the absence of dox. In contrast, 1-week exposure to dox induced an approximately 8-fold increase in thyroid mass, which regressed significantly by 72 hours, reaching normal size by 7 weeks after withdrawal (Figure 1E). As shown in Figure 2A, uninduced mice had normal thyroid histology. After 1 week on dox, all 8 mice we characterized developed clear histological features of thyroid cancer (Figure 2, B–D). The low-magnification image shown in Figure 2B shows replacement of the thyroid lobe by tumor cells with a predominantly solid growth pattern. Higher magnification reveals solid nests of tumor cells without follicular architecture or colloid formation (Figure 2C). Mitotic rate was increased, and atypical mitoses were noted (Figure 2D).

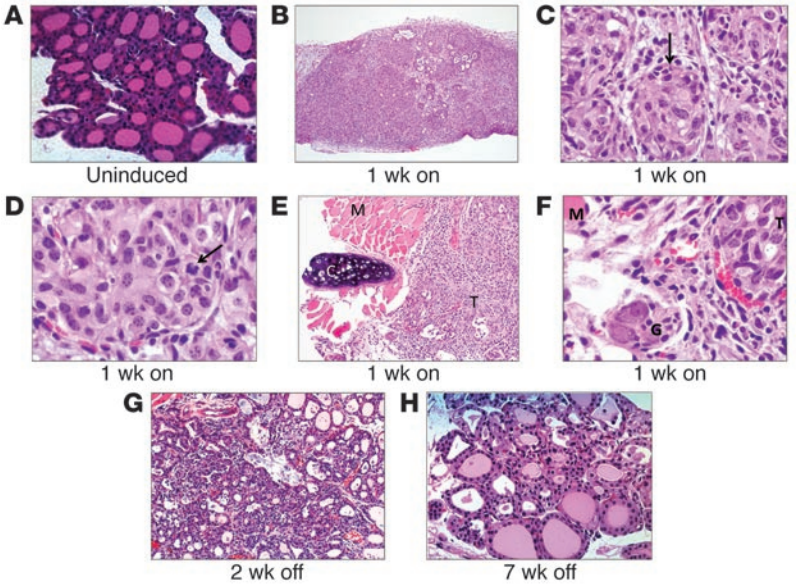

Figure 2
Tg-rtTA/tetO-BRAF^{V600E} mice develop thyroid cancer that regresses upon dox withdrawal. Representative H&E-stained sections of thyroid tissue from *Tg-rtTA/tetO-BRAF^{V600E}* fed dox chow (on) for 1 week and then regular chow (off) for the indicated times. (**A**) Uninduced *Tg-rtTA/tetO-BRAF^{V600E}* mice show normal thyroid histology with intact colloid-containing follicles. (**B**) Representative low-magnification image of a poorly differentiated thyroid cancer in a 1-week dox-treated mouse, showing predominantly a solid pattern of tumor growth and replacing the thyroid. (**C**) Higher magnification shows evidence of solid nests of tumor cells (arrow) with (**D**) atypical mitoses (arrow). (**E** and **F**) Representative images depicting extrathyroidal extension in the poorly differentiated thyroid tumors. M, muscle; C, cartilage; T, tumor; G, ganglion. (**G**) Thyroid hyperplasia without malignant features 2 weeks off dox. (**H**) Histologically normal thyroid 7 weeks after dox withdrawal. Original magnification, ×100 (**A**, **H**); ×20 (**B**, **E**, **G**); ×200 (**C**, **F**); ×400 (**D**).

Additionally, the tumor cells had characteristic nuclear features suggestive of human PTC, including nuclear enlargement, crowding and overlapping, irregularity of nuclear contours, and occasional nuclear grooves. Three of eight mice with poorly differentiated thyroid cancers also showed extrathyroidal extension of the tumor (Figure 2, E and F). There were no lymph node or distant metastases observed in these animals.

These changes regressed dramatically upon withdrawal of dox. Thus, 2 weeks after transgene deinduction, the thyroid glands were either histologically normal or had hyperplastic features (Figure 2G), and by 7 weeks. all mice had normal thyroid histology (Figure 2H). Table 1 summarizes the detailed histopathological features of thyroid tissues in groups of mice at the indicated times on or off dox.

Thyroid cancer cell growth suppression and apoptosis after BRAF^{V600E} expression is switched off. One week after dox induction of oncogenic BRAF there were nested clusters of phospho-ERK–positive–stained (p-ERK–positive–stained thyroid cells, with no identifiable follicular structures, which were surrounded by dense stroma. Two weeks after dox removal, follicular structures reappeared, and cells no longer stained for p-ERK (Figure 3A). BRAF activation was associated with a marked increase in mitotic index, as determined by Ki-67 staining, which reversed upon withdrawal of dox (Figure 3, A and B). Given the magnitude and short time frame of the decrease in thyroid tumor burden after withdrawal of oncogenic BRAF, we next determined whether the tumor cells were eliminated by apoptosis. As shown in Figure 4, A–C, this was indeed the case, as cells within the center of the thyroid tumor clusters were positive on TUNEL assays and for cleaved caspase-3 immunostaining. Increased apoptosis was observed within 72 hours of dox withdrawal and was no longer detectable by 2 weeks. This is consistent with a spatially restricted wave of apoptosis, ultimately resulting in the restoration of follicular structure.

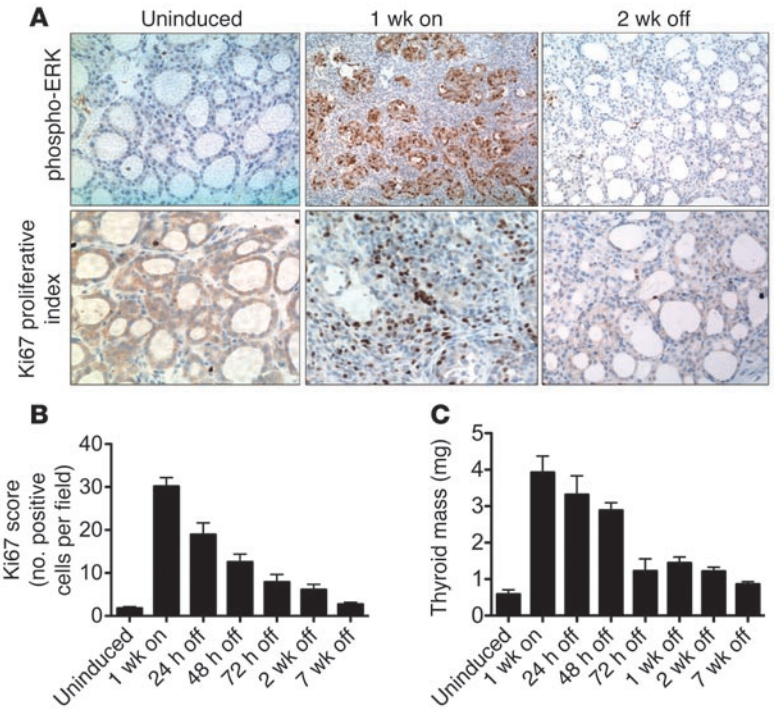

Figure 3
Reversible MAPK activation and cell proliferation in dox-treated *Tg-rtTA/tetO-BRAF^{V600E}* mice. Representative FFPE (formalin fixed paraffin embedded) sections of thyroid tissue of *Tg-rtTA/tetO-BRAF^{V600E}* mice that were untreated (uninduced), fed with dox for 1 week (1 week on), or fed with dox for 1 week followed by regular chow for 2 weeks (2 weeks off). (**A**) IHC staining for p-ERK and Ki67. Original magnification, ×100 (p-ERK, top panels); ×200 (Ki67, bottom panels). (**B**) Ki67 index at the indicated time points. Data represent manual counts of 3 high-power fields per mouse ($n = 6$ mice). (**C**) Thyroid weight of age-matched male *Tg-rtTA/tetO-BRAF^{V600E}* mice on or off dox for the indicated times. Bars represent mean ± SEM of $n \geq 8$ per time point.

Table 1
Summary of histological features of $BRAF^{V600E}$-induced thyroid tumors

Experimental group	Histopathology				
	Normal	Benign/ hyperplasia	PTC	PDTC	ETE
Uninduced	8/8	–	–	–	–
1 week on	–	–	1/8	7/8	3/8
72 hours off	–	4/8	1/8	3/8	–
1 week off	–	2/9	4/9	3/9	–
2 weeks off	7/12	5/12	–	–	–
7 weeks off	4/8	4/8	–	–	–

PTC, papillary thyroid cancer; PDTC, poorly differentiated thyroid cancer; ETE, extrathyroid extension.

dox induction of $BRAF^{V600E}$ reversibly impairs thyroid gene expression and function. As shown in Figure 5A, 1 week of dox resulted in near complete loss of sodium-iodide symporter (Nis), thyroglobulin (Tg), thyroid peroxidase (Tpo), and thyroid-stimulating hormone receptor (TshR) expression. The global downregulation of thyroid-specific genes suggested that oncogenic BRAF was likely interfering with expression of key regulatory factors required for their transcription. Indeed, *Pax-8*, *Ttf-2*, and, to a lesser extent, *Ttf-1* mRNA were profoundly downregulated after 1 week of dox (Figure 5A). Accordingly, serum T4 and thyrotropin (TSH) levels showed that these mice became hypothyroid within 48 hours of dox administration. When dox was discontinued, the expression of thyroid-specific genes was gradually restored, with consequent normalization of thyroid function (Figure 5, A and B).

Effects of small-molecule MAPK pathway inhibitors in Tg-rtTA/tetO-$BRAF^{V600E}$ mice. This model of reversible, BRAF-dependent thyroid cancer provides a powerful system for investigating the therapeutic properties of small-molecule kinase inhibitors. MEK inhibitors, such as the allosteric antagonist PD0325901, have been shown to be potent suppressors of growth of human cancer cell lines with *BRAF* mutations (26), including those derived from thyroid tumors (22, 23). We determined whether treatment of dox-induced thyroid cancers with PD0325901 recapitulated the effects of dox withdrawal on thyroid growth, histology, and gene expression. As shown in Supplemental Figure 2, treatment of $BRAF^{V600E}$-induced thyroid cancers with 25 mg/kg/d PD0325901 failed to induce tumor regression or restore thyrocyte gene expression and did not return mice to a euthyroid state.

We next examined the pharmacodynamics of PD0325901 on MAPK signaling in thyroid tissues of mice exposed to dox for 1 week. As shown in Figure 6, administration of a single 25 mg/kg dose resulted in a greater than 90% inhibition of p-ERK at 6 hours, which was followed by a rebound at 24 hours, perhaps explaining the lack of effect on tumor phenotype and on thyroid gene expression of prolonged treatment with this dose schedule. We then explored the pharmacodynamic effects of administering the compound at 12.5 mg/kg every 12 hours. Although we observed only an approximately 60% inhibition of MAPK signaling as determined by p-ERK, this was more sustained throughout the 24-hour time course. We therefore did further efficacy studies with the new PD0325901 schedule; however, due to toxicity, these experiments had to be terminated after 6 days.

Besides MEK inhibitors, we also tested the effects of the $BRAF^{V600E}$-selective inhibitor PLX4720, which has potent inhibitory effects on BRAF-positive melanoma cell lines and animal models (28) and in human thyroid cancer cell line xenografts (24, 25). The PLX4720 analog PLX4032 (vemurafenib) has induced remarkable responses in patients with aggressive BRAF-positive melanomas (29). After testing multiple doses of PLX4720 by oral gavage (data not shown), we used a PLX4720-impregnated chow (417 mg/kg PLX4720), which delivered a high serum concentration of the compound (>70 μg/ml)

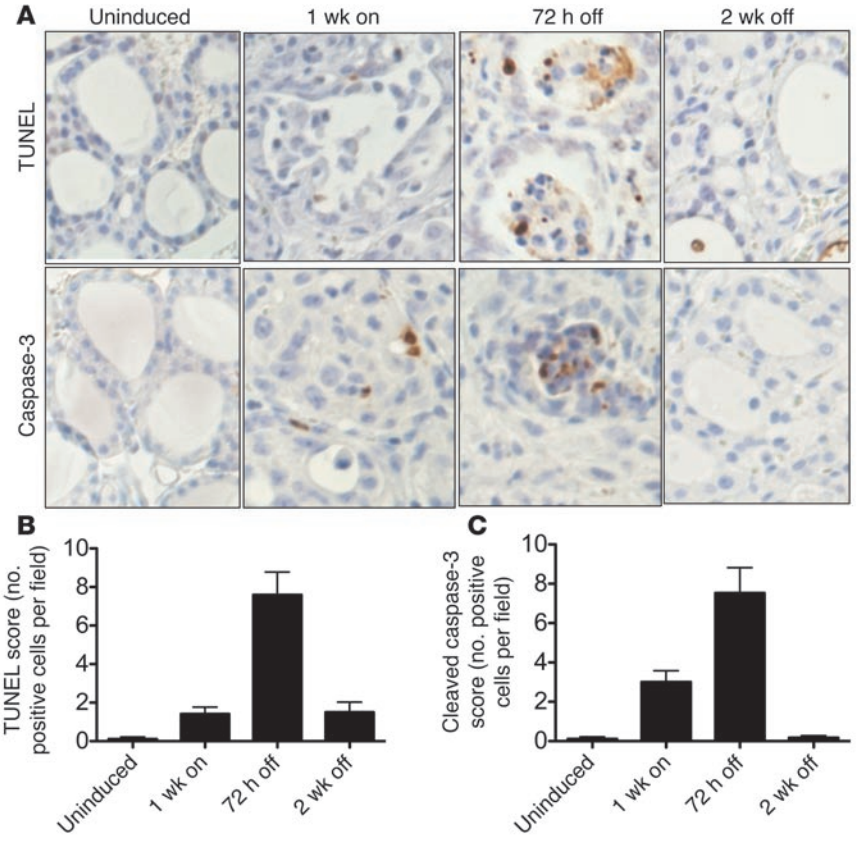

Figure 4
Withdrawal of *$BRAF^{V600E}$* expression leads to thyroid cancer cell apoptosis. (**A**) Representative FFPE sections of thyroid tissues from *Tg-rtTA/tetO-$BRAF^{V600E}$* fed dox for 1 week (on) and then regular chow (off) for the indicated times, assayed by TUNEL (top) and cleaved caspase-3 (bottom). There was a modest increase in apoptotic cells at 1 week on dox, which were scattered throughout the thyroid tumor specimen. In contrast, the brown-red staining cells were localized within the center of the cancer cell clusters 72 hours after dox withdrawal. Original magnification, ×400 (top panels); ×400 (bottom panels). (**B** and **C**) Quantification of TUNEL and cleaved caspase-3 (+) cells at the indicated times. Data are shown as mean ± SEM and correspond to manual counting of 3 high-power fields/mouse (n = 6).

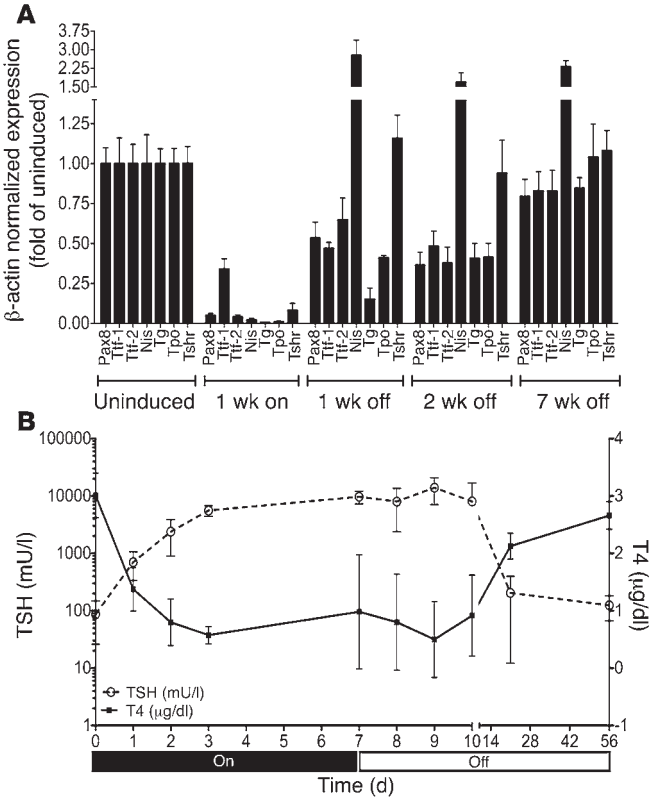

Figure 5
Effect of oncogenic BRAF on thyroid-specific gene expression and thyroid function. (**A**) *Tg-rtTA/tetO-BRAF*^{V600E} mice were fed dox chow (on) for 1 week and then regular chow (off) for the indicated times. Bars show results of qRT-PCR of *Pax8*, *Ttf1*, *Ttf2*, *Nis*, *Tg*, *Tpo*, and *Tshr* mRNA after normalization to β-actin. Data are expressed as mean ± SEM compared with uninduced controls. (**B**) Serum TSH and total T4 levels in mice on and off dox for the indicated periods. Left *y* axis, dashed line, serum TSH mU/l; right *y* axis, solid line, serum T4 μg/dl. Data are presented as the mean ± SEM.

throughout the course of treatment. The effects of PLX4720 on MAPK signaling were evaluated by immunohistochemistry (IHC) instead of Western blotting, because RAF inhibitors can evoke reciprocal changes on tumor (BRAF-positive) versus stromal (BRAF-negative) cells (30). As shown in Supplemental Figure 3C, PLX4720 inhibited p-ERK robustly in the tumor cells.

We verified that the expression of the BRAF transgene was not affected by either drug as determined by quantitative PCR (qPCR) (not shown). These treatments did not reduce the size of the thyroid glands or attenuate the histological appearance of the PTC induced by dox (Supplemental Figure 3, A and B). However, both drugs markedly inhibited the proliferative index, with a more profound effect seen in the PLX4720-treated animals (Figure 7A). Combination studies using once-a-day 25 mg/kg PD0325901 with PLX4720 chow resulted in unacceptable toxicity and could not be pursued.

Effects of dox withdrawal, PD0325901, and PLX4720 on thyroid-specific gene expression and ^{124}*I-iodine uptake in oncogenic BRAF-induced thyroid cancers*. Withdrawal of dox for 2 weeks partially restored thyroid function in *Tg-rtTA/tetO-BRAF*^{V600E} mice (Figure 5B). A similar, but more attenuated, recovery trend was observed in mice treated with either PD0325901 or PLX4720 (Figure 7B). Expression of thyroid-specific genes was also partially restored by treatment with the compounds, although only to a moderate extent (Figure 7C). *Nis* mRNA expression, in particular, was only increased modestly (PLX4720 > PD0325901). We also examined Nis protein expression and localization by IHC. As shown in Figure 8, normal thyroid follicular cells of uninduced mice showed basolateral plasma membrane Nis immunoreactivity, which was completely lost upon 1 week induction of oncogenic BRAF. Stopping dox for 1 week fully restored Nis plasma membrane immunoreactivity, which appeared greater in intensity than at baseline, consistent with the *Nis* mRNA data (Figure 5A). Nis protein expression and appropriate localization also recovered upon treatment with PLX4720 and, to a lesser extent, PD0325901.

Indeed, there was a marked recovery of thyroidal incorporation of ^{124}I-iodide in vivo in response to the MAPK pathway inhibitors. Representative microPET images (Figure 9A) and quantitative dosimetry calculations (Figure 9B) both demonstrated a dramatic increase in ^{124}I-iodide uptake by both compounds to levels that approximated those seen after dox withdrawal and corresponding to approximately 40% of iodine incorporation of normal thyroid tissue. However, analysis of the time-activity curves showed a biological half-life of 43.4 ± 8 hours in mice 1 week after dox with-

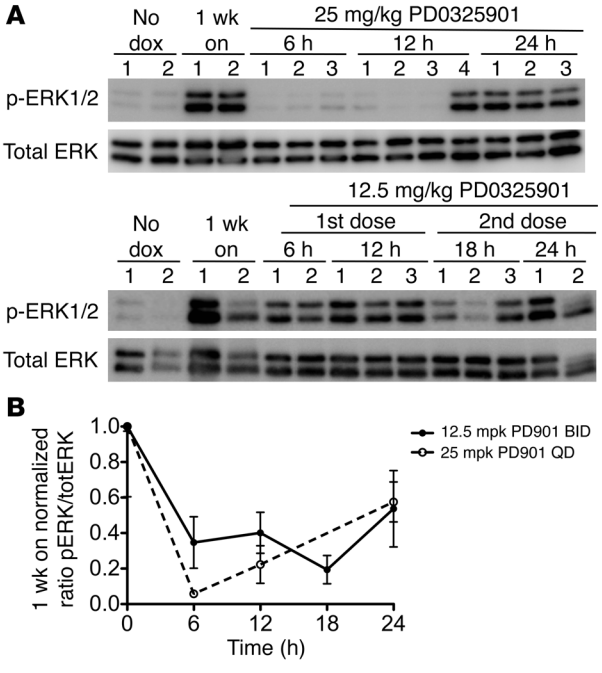

Figure 6
Pharmacodynamic effects of the MEK inhibitor PD0325901 in thyroid cancers of *Tg-rtTA/tetO-BRAF*^{V600E} mice. (**A**) Western blot of thyroid tissue lysates for p-ERK and total ERK from mice treated either with PD0325901 as a single dose of 25 mg/kg (upper panel) or with 12.5 mg/kg every 12 hours (lower panel). The number of replicates is specified under each time point. (**B**) Quantification of the p-ERK/total ERK ratio at the indicated time points shown as fold change of 1-week dox-treated animals: dashed line, 25 mg/kg PD0325901 given at time 0; solid line, 12.5 mg/kg PD0325901 given at 0 and 12 hours. Data are presented as mean ± SEM.

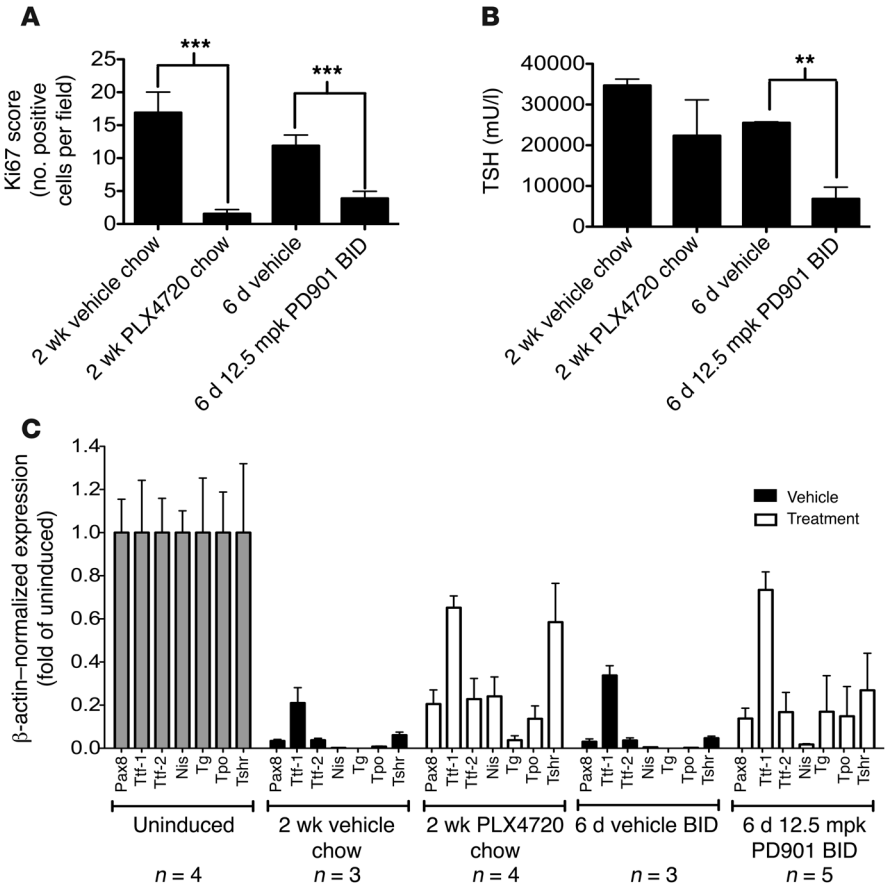

Figure 7
Activity of small-molecule inhibitors of the MAPK pathway in *BRAF*^{V600E}-induced thyroid tumors. Mice were pretreated for 1 week with dox and then either fed with PLX4720 or vehicle chow for 2 weeks or given PD0325901 (12.5 mg/kg every 12 hours) or vehicle for 6 days in the continued presence of dox. (**A**) Ki67 index of thyroid sections from mice treated with or without the indicated drug. The proliferative index was significantly decreased by both compounds. ***$P < 0.001$. (**B**) Serum TSH levels of mice treated with or without the indicated compounds. TSH levels were significantly lower in mice treated with PD0325901. **$P < 0.01$. (**C**) Expression levels of the indicated genes normalized to β-actin as determined by qRT-PCR in the indicated conditions. Gray bars indicate expression levels in mice not treated with dox. The number of animals per group is specified in the graph. Data are presented as the mean ± SEM.

drawal, compared with 26.7 ± 9.5 hours after PLX4720 treatment ($P < 0.01$) (Tables 2 and 3, and Figure 9C). Of note, in the latter experiment, PLX4720 was given by oral gavage, which resulted in a lower uptake at 24 hours compared with that of mice given drug-impregnated chow (Figure 9B), likely because of the differential bioavailability and pharmacokinetics of the drug between the 2 routes of administration.

BRAF switch-off or PLX4720 treatment renders thyroid cancer cells susceptible to RAI-induced DNA damage and apoptosis. We next investigated whether genetic or pharmacological inhibition of mutant BRAF sensitized cells to radiation delivered through a therapeutic dose of ^{131}I-iodide. Since restoration of thyroid-specific gene expression, including of Nis, was greater in mice treated with PLX4720 than PD0325901 (Figures 7 and 8), we focused on mice treated with this compound. After treatment of mice with 3 mCi ^{131}I-iodide, there was a marked increase in γH2AX staining, peaking at 24 hours, which was greater after dox withdrawal compared with that in drug-treated mice. Accordingly, there was an increased frequency of apoptosis in both conditions, as determined by caspase staining and TUNEL assays, with drug-treated animals showing a significant, but weaker, effect (Figure 10).

Discussion

Tetracycline-inducible transgenic models of oncogenes such as MYC, RAS, and EGFR in different cell types helped establish the concept of oncogene addiction in vivo by showing that deinduction of the initiating oncoprotein causes tumor regression (16–19, 31). Our objective in this study was to demonstrate that conditional BRAF expression in thyroid cells of adult mice was sufficient to induce tumorigenesis and that the cancer cells required the continued presence of the oncoprotein for tumor maintenance. In addition, we wanted this information to serve as the gold standard to evaluate the therapeutic effects of selective inhibitors of BRAF signaling, particularly focusing on their effects on iodine transport and retention, since treatment with RAI is a key therapeutic modality in this disease.

One of the striking aspects of the tumor phenotype was the very short latency required for transformation, which occurred nonfocally throughout the entire thyroid gland. Mice expressing endogenous levels of Braf^{V600E} as of E14.5 develop histological features of PTC beginning at approximately 3 weeks postnatally (32), whereas adult-onset activation of a latent knockin *Braf* allele generates PTCs after approximately 6 months (33). The more rapid onset seen in the current study may be due to overexpression of the oncogene. Braf-induced thyroid tumor initiation requires TSH action (32), but once established, further growth and viability are largely independent of TSH. This is also likely the case after dox induction of oncogenic BRAF, because the TSH receptor is rapidly and profoundly downregulated by BRAF in this model, thereby rendering the thyroid cells unresponsive to the ligand. Oncogenic BRAF also impairs responses to TSH at steps distal to the TSH receptor within 48 hours, including the ability of its intracellular signaling effector cAMP to induce *Nis* mRNA (14). In contrast, conditional activation of an endogenous mutant *Braf* allele in melanocytes primarily induces benign nevi, which express markers of senescence and have a low mitotic rate. Malignant melanomas

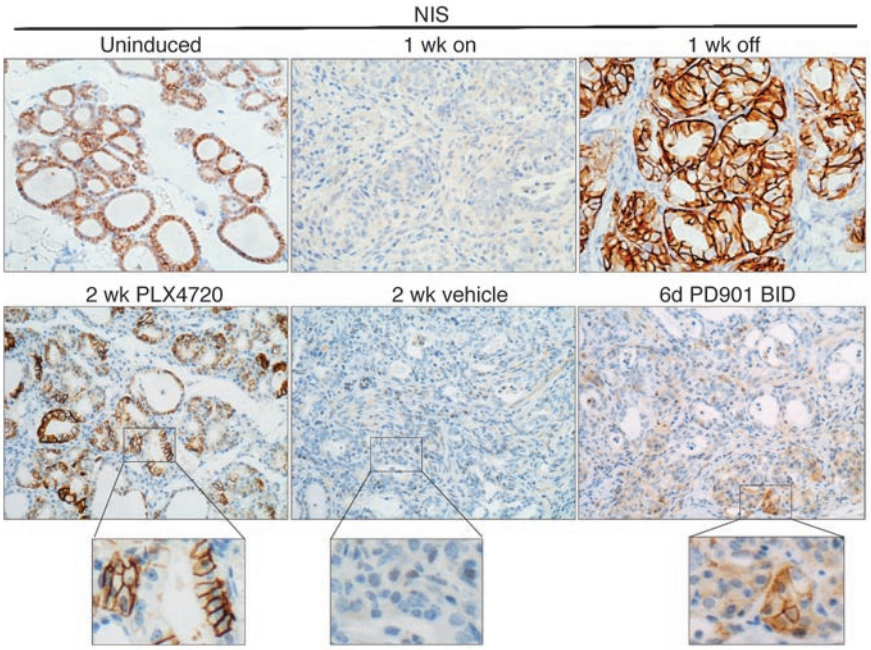

Figure 8
Nis protein expression and localization are restored upon dox withdrawal or treatment with MAPK pathway inhibitors. Nis IHC in representative sections of thyroid tissue of mice in the indicated conditions. Original magnification, ×200; ×400 (insets).

do ultimately arise, but only after a prolonged latency, suggesting a requirement for cooperating genetic events (21). This is not likely the case for the malignant phenotype observed in our model, because it manifests ubiquitously throughout the entire thyroid gland after a short latency. However, we did not observe nodal or distant metastases here or in mice with thyroid-specific expression of a latent Braf allele (32), suggesting that other oncogenic hits are needed for metastatic spread.

The $BRAF^{V600E}$-induced PTCs closely recapitulate the histology of BRAF-positive advanced human thyroid cancer, with classic PTC architecture, presence of tall cell features, and evidence of extrathyroidal extension, consistent with their proclivity for invasion (3, 15). Upon dox withdrawal, thyrocyte apoptosis occurs in an organized pattern, beginning within the center of the tumor micronodules and radiating outward, leaving behind thyroid cells in the periphery of the nodule that appear to secrete Tg into the apical lumen. The restoration of gland architecture after oncogenic withdrawal is remarkable, but not unprecedented. Similar observations have been reported in MYC- and K-RAS–induced murine breast acinar 3D primary cultures following deinduction of oncoprotein expression. This was associated with clearance by caspase-3–mediated apoptosis of cells within the center of the disorganized mammospheres, leaving behind repolarized acinar structures (34).

Approximately 70% of human PTCs are associated with mutually exclusive mutations of *RET* or *TRK*, *RAS* (*NRAS* > *HRAS* > *KRAS*) or *BRAF* (2, 35, 36). The oncoproteins encoded by these genes share the common property of constitutively activating MAPK signaling, which has been taken as evidence supporting a critical role of this pathway in the pathogenesis of the disease. The expression of many of the genes required for thyroid hormone biosynthesis (e.g., NIS, TG, TPO) is particularly sensitive to the activity of the MAPK pathway. This has been demonstrated in PCCL3 cells, a rat thyroid cell line that retains most of the differentiated properties of normal thyrocytes, in which conditional activation of RET/PTC1 or RET/PTC3 downregulates expression of Nis, Tg, and Tpo (37, 38). This effect was abolished upon deletion of RET-Y1062, which is required to couple to Shc-Sos-Ras. The inhibitory effect was recapitulated by conditional expression of oncogenic RAS or of constitutively active MEK and restored by treatment with MEK inhibitors (39). Accordingly, conditional expression of oncogenic BRAF has a similar effect on these cells (14).

The mechanism or mechanisms by which constitutive MAPK pathway activation inhibits NIS expression have recently been clarified. BRAF activation has been proposed to induce a TGF-β autocrine loop (40), which downregulates Pax8 and evokes a Smad3-dependent inhibition of Pax8 binding to the Nis promoter (41). Interestingly, short-term pretreatment of PCCL3 cells prior to induction of $BRAF^{V600E}$ with MEK inhibitors did not restore Nis activity, whereas treatment with a TGF-β–R1 inhibitor was more effective. These results contrast with our data in mice, in which PD0325901 treatment for 6 days resulted in a clear reactivation of iodine uptake. It is possible that a longer treatment time is required to switch off both the direct and indirect consequences of MEK overactivity on Nis expression.

In this study, we used 2 compounds working at different levels of the MAPK signaling pathway to attempt to reverse the biological consequences of oncogenic BRAF activation. The exquisite reversibility of the entire phenotype by switching off the oncoprotein set the scene for establishing the comparative efficacy of drugs targeting BRAF itself or its downstream effector MEK. Neither PLX4720 nor PD0325901 resulted in regression of the papillary thyroid cancers after 2 weeks of therapy. Recent data show that in order to achieve full therapeutic benefit with RAF inhibitors, it is not sufficient merely to inhibit the MAPK pathway, but that it needs to be almost completely suppressed (42). Indeed, as opposed to the dramatic reversibility of the phenotype after dox withdrawal, treatment of thyroid cancers with 25 mg/kg/d PD0325901 failed to decrease mitotic activity or to induce tumor regression. This is likely explained by the fact that inhibition of MAPK signaling was transient with this dosing schedule. Although p-ERK inhibition was not as profoundly inhibited when mice were treated with 12.5 mg/kg of

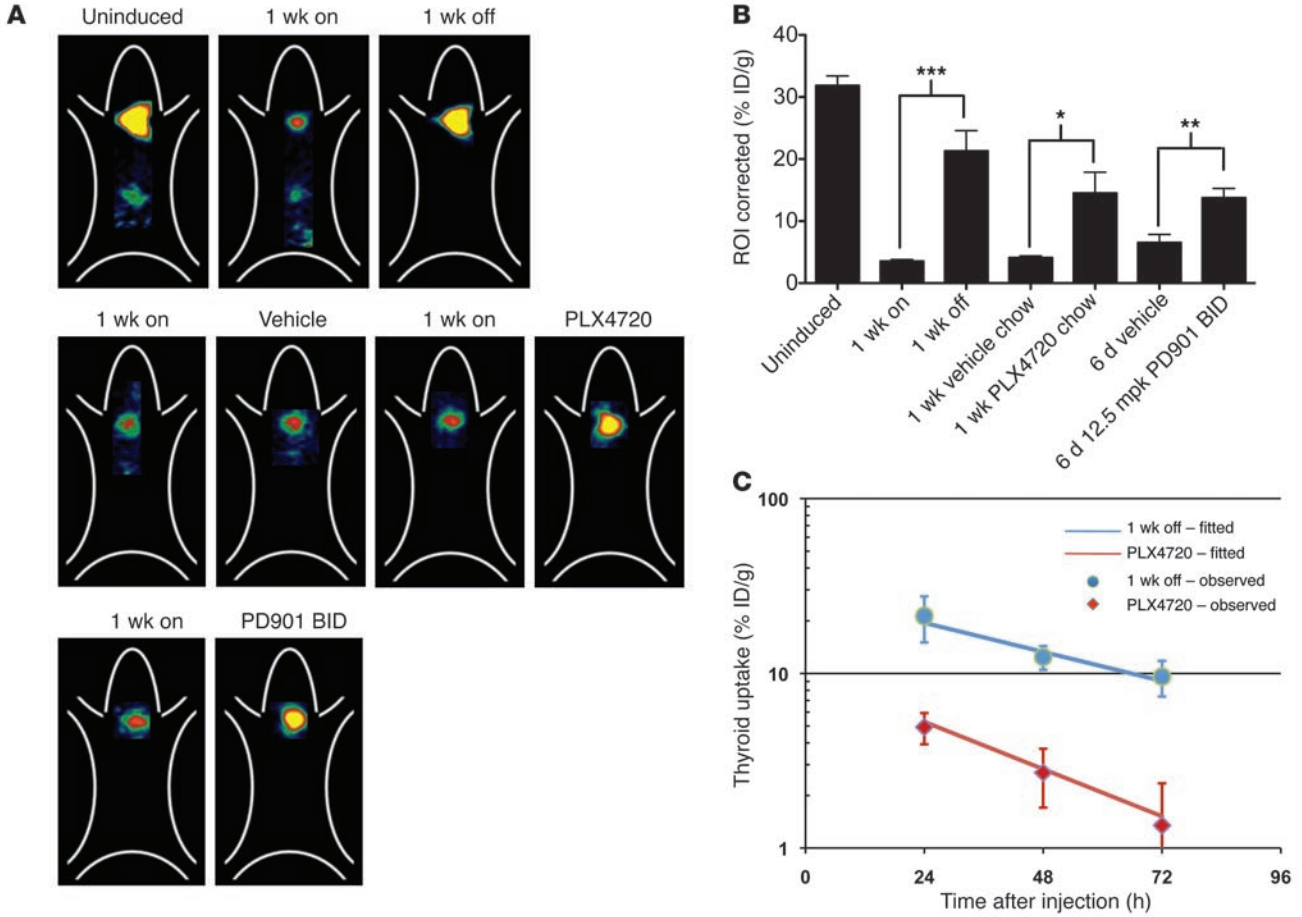

Figure 9

Recovery of thyroidal incorporation of ^{124}I-iodide in vivo in response to the MAPK pathway inhibitors. (**A**) Biodistribution of ^{124}I-iodide in thyroid tissues of *Tg-rtTA/tetO-BRAF^{V600E}* mice (coronal images parameterized in terms of %ID/g).Top panels: representative images of uninduced mice, 1 week on dox, and 1 week on followed by 1 week off dox. Middle panels: images of mice treated with dox for 1 week, followed by 1 week of vehicle chow (second panel) or PLX4720 chow (fourth panel) in the continued presence of dox. Bottom panels: PD0325901 12.5 mg/kg every 12 hours for 6 days. (**B**) Quantification of ^{124}I-iodide uptake in mice treated with the indicated conditions. *$P < 0.02$; **$P < 0.01$; ***$P < 0.001$. (**C**) Thyroid time-activity data of ^{124}I-iodide incorporation in mice after 1 week off dox or 1 week on treatment with PLX4720 given by gavage at 100 mg/kg. Biological half-life in the 2 conditions is shown in Tables 2 and 3. Data are presented as mean ± SEM.

the compound every 12 hours, the effect was more sustained, which was associated with improved responses, i.e., decreased proliferation and partial reduction of TSH levels. The fact that oncogenic BRAF was overexpressed in this model may also have contributed to the attenuated responses to small molecule MAPK pathway inhibitors as compared with dox withdrawal. Notably, the 2 drugs had a robust effect on ^{124}I-iodide incorporation, yet the recovery of *Nis* mRNA expression was modest when compared with switching off BRAF expression. This could be due in part to the continued presence of stroma in drug-treated animals, resulting in dilution of the *Nis* mRNA signal. Indeed, evaluation of NIS by IHC showed clear restoration of the symporter, which was appropriately targeted to the plasma membrane. Besides restoring iodine uptake, the striking increase in ^{124}I-iodide incorporation after drug treatment could also be due to greater iodine organification, since these compounds increased Tg and Tpo levels.

Withdrawal of dox was associated with a marked response to RAI treatment, as determined by the induction of DNA damage and cell death. Treatment with PLX4720 elicited similar, albeit weaker responses. This is likely due to lower uptake as well as a shorter half-life of the isotope in drug-treated versus BRAF deinduced animals. The retention of inorganic iodide in thyroid cells required the activity of Tpo for its incorporation into tyrosine residues and subsequently into iodoproteins. Overall, the kinase inhibitors had a more attenuated effect on restoration of Nis expression levels, as well as those of Tpo and Tg, compared with those in dox-withdrawn mice. This likely explains not only the weaker uptake, but also the shorter ^{124}I-iodide residence time after PLX4720. Indeed, after dox withdrawal, there was a 2.9-fold higher uptake as well as 1.6-fold longer biological half-life, which together predict a 4.7-fold higher radiation dose compared with that of drug-treated animals.

A clinical trial of the RAF inhibitor PLX4032 in patients with metastatic melanomas elicited spectacular clinical regressions of the disease in the large majority of cases, which were only observed in patients harboring *BRAF* mutations (29). Interestingly, 3 patients with *BRAF*-positive PTC included in the dose-escalation phase of the study also showed tumor control, including 1 patient with a partial response. The RAF inhibitor PLX4720 had a profile

Table 2
^{124}I thyroid uptake in *Tg-rtTA/tetO-BRAF^{V600E}* mice

Time after injection (h)	Uptake (%ID/g) Fitted values 1 week off	Fitted values PLX4720	Measured values 1 week off Mean	1 week off SEM	PLX4720 Mean	PLX4720 SEM
24	19.5	5.3	21.28	6.23	4.93	0.13
48	13.3	2.8	12.42	1.92	2.70	0.44
72	9.1	1.5	9.58	2.21	1.35	0.38

of activity similar to that of PLX4032 and showed the most promising effects on RAI incorporation in this mouse model. Together, these data show that the BRAF-induced inhibition of iodine incorporation is a reversible process and that optimal inhibition of MAPK signaling represents a promising strategy to achieve this.

BRAF mutations are overrepresented in RAI-refractory thyroid cancers (6), and these have lower expression of TG, TPO, and NIS compared with PTCs harboring either RAS or RET/PTC (43). Accordingly, they are more refractory to ^{131}I-iodide therapy (4). Hence, patients with *BRAF* (+) PTCs would be ideally suited for therapeutic trials with MAPK pathway inhibitors to restore RAI treatment efficacy, in particular with relatively selective BRAF inhibitors. However, it should be noted that tumors with *RET/PTC* rearrangements or *RAS* mutations also have comparatively lower RAI uptake than normal thyrocytes. As these oncoproteins inhibit NIS, TG, and TPO expression in a MEK-ERK–dependent manner (39), it is likely that MAPK pathway inhibitors may also have a beneficial effect on iodine transport and organification in thyroid cancers harboring these defects.

Methods

Generation of Tg-rtTA and tetO-BRAF^{V600E} mice. The reverse tetracycline transactivator rtTA2s-M2 cDNA (a gift from Hermann Bujard, Heidelberg University, Heidelberg, Germany) was cloned into the *Eco*RI/*Bam*HI site of pSG5, downstream of the β-globin intron and upstream of a polyadenylation sequence (Supplemental Figure 1A). This construct was then cloned downstream of the bovine Tg promoter into the *Cla*I/*Sal*I site of pSKbTg to generate the *Tg-rtTA* vector. The *tetO-BRAF^{V600E}* vector was previously described and consists of 7 repeats of a tetracycline operator sequence and a minimal cytomegalovirus promoter cloned upstream of a myc-tagged human BRAF^{V600E} cDNA (Supplemental Figure 1A).

The *Not*I/*Sal*I fragment containing rtTA2s-M2 cDNA or the *ApaL*I fragment containing the myc-tagged *tetO-BRAF^{V600E}* cDNA was injected separately into fertilized FVB/N mouse eggs, which were then implanted into pseudopregnant female mice. Integration of the transgene in the pups was confirmed by PCR and Southern blotting. Individual *Tg-rtTA* founder lines were assessed for rtTA expression by qRT-PCR of thyroid tissue. The founder line with the highest thyroid-specific expression of rtTA (line 30) was crossed with 3 individual *tetO-BRAF^{V600E}* founders (lines 3, 26, and 27). The *Tg-rtTA* (line 30) cross with *tetO-BRAF^{V600E}* (line 26) was found to have the highest dox inducibility and least leaky expression of the transgene and was therefore selected for all further studies (Supplemental Figure 1, B–D).

Mouse genotyping was performed on tail DNA, isolated with the DNeasy 96 Blood and Tissue Kit (QIAGEN) according to the manufacturer's instructions. The dox was administered to *Tg-rtTA/tetO-BRAF^{V600E}* mice via dox-impregnated food pellets (2500 ppm; Harlan-Teklad). Mice were placed on dox at 6 to 13 weeks of age (median of 8 weeks) for the indicated times. Mice were euthanized according to institutional guidelines; thyroid lobes were extracted and either snap-frozen for RNA and protein analysis or fixed in 4% paraformaldehyde for histological and immunohistochemical analyses.

Real-time RT-PCR. Thyroid lobes were surgically removed, weighed, and immediately snap-frozen in liquid N_2. RNA was isolated using RNA PrepEase Kit (USB Corporation), and 0.3 μg was reverse transcribed with SuperScript III (Invitrogen) in the presence of random hexamers to generate cDNA. qRT-PCR was done using QuantiTect SYBR Green PCR Kit (QIAGEN) using the primer pairs specified in Supplemental Table 1. The cycle threshold values for β-actin and the target gene product were determined using Mastercycler ep realplex (Eppendorf) and used to calculate the normalized relative expression using the QGENE program (44).

Western blotting. Fresh frozen thyroid tissues were homogenized in RIPA lysis buffer (20 mM Tris [pH 7.4], 135 mM NaCl, 2 mM EDTA, 1% Triton X-100, 25 mM β-glycerophosphate, 1 mM sodium orthovanadate, 1 mM NaF, 1 mM phenylmethylsulfonyl fluoride, 10 μg/ml pepstatin, and 10 μg/ml aprotinin) and incubated for 30 minutes at 4°C. Cell debris were removed by centrifugation at 14,000 *g* for 20 minutes at 4°C, and the supernatant protein concentration was determined by BCA assay (Pierce). Equal amounts of total protein were resolved by SDS-PAGE, transferred to PVDF membranes, and immunoblotted with the indicated primary antibodies. Membranes were hybridized with the following primary antibodies: Raf-B (C-19, sc-166), 1:1000; ERK1 (K-23, sc-94), 1:2000 (Santa Cruz Biotechnology Inc.); p-MEK1/2 serine 217/221 (#9121), 1:500; p-p44/42 MAPK threonine 202/tyrosine 204) (Erk1/2) (#9101), 1:1000; MEK1 (#9124), 1:1000; and α-tubulin (#2144), 1:2000 (Cell Signaling Technology). Membranes were hybridized with species-specific HRP-conjugated antibodies, goat anti-mouse IgG-HRP (sc-2031), 1:2000, and goat anti-rabbit IgG-HRP (sc-2030), 1:2000 (Santa Cruz Biotechnology Inc.). Bands were visualized with enhanced chemiluminescence (GE Healthcare Biosciences) as directed by the manufacturer.

Histology and IHC. Thyroid tissues were immediately placed in 4% paraformaldehyde and incubated overnight at 4°C. The next day, tissue was washed twice with PBS for 30 minutes followed by a single 30-minute 50% ethanol wash. The fixed tissue was then placed in 70% ethanol, paraffin embedded, and sectioned into 4-μm paraffin sections. H&E-stained slides were evaluated by a board-certified pathologist (R. Ghossein). Mouse thyroid sections were deparaffinized and immunostained with antibodies to Ki67 (VP-K451; Vector Laboratories), p-ERK (#9101; Cell Signaling Technology), cleaved caspase-3 (Asp175) (#9661; Cell Signaling Technology), and human NIS (a gift from Nancy Carrasco, Albert Einstein College of Medicine, New York, New York, USA) at the Memorial Sloan-Kettering

Table 3
Monoexponential fits of microPET-derived thyroid time-activity data

	Zero-time intercept (%ID/g)	Biological half-time (h)
1 week off		
Mean	28.6	43.4
SD	7.9	8.0
PLX4720		
Mean	9.9	26.7
SD	2.0	9.5

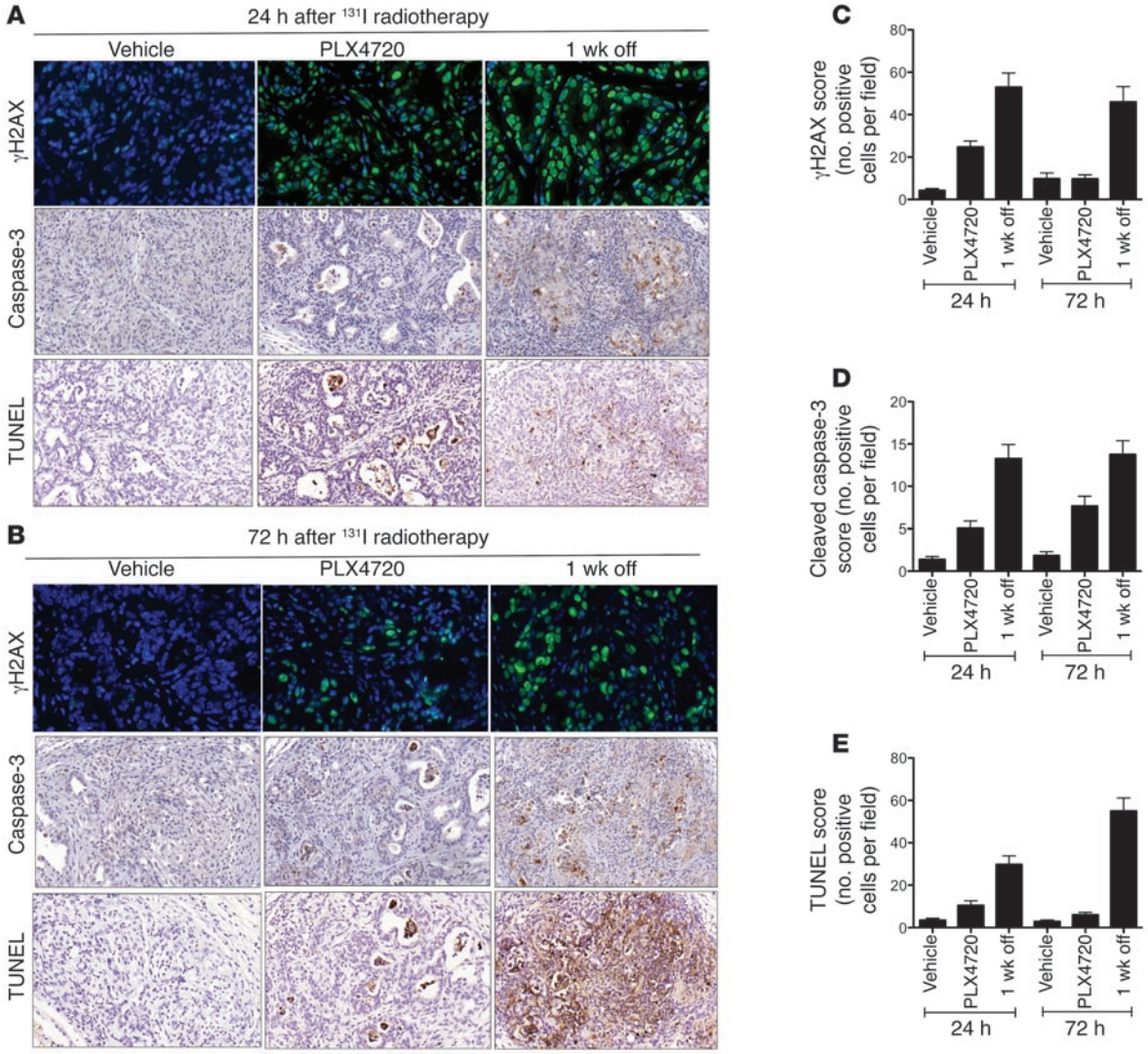

Figure 10
Radioiodine therapy after dox withdrawal or PLX4720 treatment in *BRAF*^{V600E}-induced thyroid tumors. *Tg-rtTA/tetO-BRAF*^{V600E} mice were pretreated for 1 week with dox, then either fed with regular chow alone (1 week off) or continued on dox for an additional week in the presence of either vehicle or PLX4720 chow. After 2 weeks, all mice were injected with 3 mCi ^{131}I-iodide, and mice were sacrificed 24 and 72 hours after injection. Representative FFPE sections of thyroid tissues from *Tg-rtTA/tetO-BRAF*^{V600E} at (**A**) 24 hours and (**B**) 72 hours after ^{131}I-iodide injection stained as follows: top panels, γH2Ax (green) and DAPI (blue); middle panels, cleaved caspase-3; or bottom panels, TUNEL. Original magnification, ×1000 (top panels); ×400 (middle panels); ×400 (bottom panels). (**C**–**E**) Quantification of γH2Ax, cleaved caspase-3, and TUNEL(+) cells at the indicated times. Data are mean ± SEM, and correspond to manual counting of ≥ 3 high-power fields/mouse (n = 3).

Cancer Center Molecular Cytology Core Facility. For γH2AX stains, tissue sections were incubated with a mouse monoclonal antibody against γH2AX (Millipore) and Alexa Fluor 488–conjugated antibody to mouse immunoglobulin (Invitrogen). The fluorochromes were visualized with Mirax Scan (Zeiss). Images were exported as tif files using Panoramic Viewer (3D Histech), and γH2AX-positive cells were manually counted at ×1000 magnification.

TUNEL assay. DNA fragmentation was detected by labeling free 3′-OH termini with FITC-labeled dUTP. Paraffin-embedded thyroid sections were de-waxed, rehydrated, and incubated with 20 μg/ml proteinase K for 15 minutes at 37°C. Slides were subsequently washed with PBS and refixed with 4% paraformaldehyde. Endogenous peroxidase activity was quenched by treatment with 1% hydrogen peroxidase and blocking with avidin and biotin. After equilibration with terminal deoxynucleotidyl transferase (TdT) buffer (30 mM Tris·HCl, pH 7.2, 140 mM sodium cacodylate/1 mM cobalt chloride) for 5 minutes at room temperature, the slides were incubated in 70 μl of TdT buffer with 100 units of TdT (#3333574; Roche Applied Sciences) and 5 μM biotin-dUTP (#1093070; Roche Applied Sciences) at 37°C for 1 hour. The reactions were terminated with 2× SSC buffer (0.3 M NaCl/0.03 M sodium citrate) for 15 minutes at room temperature. Apoptotic sites were revealed by immunoperoxidase using the Vectastain ABC Kit (Vector Laboratories Inc.), with 3,3′-diaminobenzidine as the substrate.

Radioimmunoassay for serum TSH and levothyroxine. Blood from mice was collected immediately after euthanasia with CO_2 and centrifuged at maximum speed at 4°C for 15 minutes. Serum was removed and stored

at –70°C until assayed. Serum TSH levels were determined as previously described (45). The lower limit of detection for TSH in this assay was 10 mU/l. Samples with high TSH levels were diluted with TSH-deficient mouse serum so that all measurements were within the linear part of the standard curve. The serum levels of total thyroxine were measured using an antibody-coated tube radioimmunoassay (RIA) (Siemens Medical Solutions Diagnostics) adapted for mouse serum. The lower limit of detection for levothyroxine (L-T4) in this assay was 0.25 μg/dl.

RAI (^{124}I-iodide) thyroid uptake and PET imaging. PET imaging was performed using an R4 microPET scanner (Concorde Microsystems) with Na^{124}I produced on the MSKCC EBCO TR 19-9 (Advanced Cyclotron Systems Inc.) using 16-MeV protons on a tellurium-124 target (46). Mice were injected via tail vein with 1.7–2.0 MBq (45–55 uCi) of Na^{124}I. Mice were imaged 24, 48, and 72 hours later under inhalational isoflurane anesthesia (Forane; Baxter Healthcare) at 1 l/min. List-mode data were acquired for 5 minutes using an energy window of 250–750 keV and a coincidence timing window of 6 nsec, histogrammed into 2D projected data by Fourier rebinning, and reconstructed by filter back-projection using a cut-off frequency equal to the Nyquist frequency. The image data were normalized to correct for nonuniformity of response of the PET, dead-time count losses, ^{124}I positron branching ratio, and physical decay to the time of injection, but no attenuation, scatter, or partial-volume averaging correction was applied. An empirically determined system calibration factor (in units of [μCi/ml] / [cps/voxel]) was used to convert reconstructed voxel count rates to activity concentrations. The resulting image data were then normalized to the administered activity to parameterize images in terms of the percentage of the injected dose per gram of tissues (%ID/g). Manually drawn 2D regions of interest (ROIs) or 3D volumes of interest (VOIs) were used to determined the %ID/g (decay corrected to the time of injection) in various tissues. Image visualization and analysis were performed using ASIPro VM software (Concorde Microsystems).

RAI therapy. Preparation, dilution, and injection of ^{131}I-NaI were performed in a designated Comecer (Castelle Bolognese) radioisotope fume hood. Approximately 111 MBq (3 mCi) of USP-grade ^{131}I-NaI (Nuclear Diagnostic Products) in 200–300 μl isotonic saline was administered to each mouse via tail-vein injection. Mice were placed in a designated radioactive animal holding facility. Ex vivo measurements of ^{131}I-NaI activity within the thyroid gland (in %ID/g) were performed by harvesting the thyroid at necropsy, weighing the tissue specimen, and assaying it in a scintillation well counter calibrated for ^{131}I-iodide (Wizard 3 Gamma Counter; PerkinElmer).

Treatment of mice with MEK or RAF inhibitors. The indicated concentration of the allosteric MEK inhibitor PD0325901 was administered by oral gavage as a suspension in 0.5% HPMT (hydroxypropyl methyl cellulose) containing 0.2% (v/v) Tween 80. *Tg-rtTA/tetO-BRAF^{V600E}* mice were fed 2500 ppm dox for 1 week. Thereafter, mice were randomized to receive either HPMT vehicle or PD0325901. PD0325901 was administered at 25 mg/kg once a day or 12.5 mg/kg every 12 hours by oral gavage in a volume of 100 μl using a sterile animal feeding needle for the indicated times.

PLX4720 (Plexxikon) was administered as a drug-admixed chow with a nominal drug load of 417 mg/kg. For this experiment, *Tg-rtTA/tetO-BRAF^{V600E}* mice were fed with chow containing 2500-ppm dox for 1 week and then randomized to receive either PLX4720 or vehicle chow for 2 weeks. During the 2-week drug-treatment period, dox was administered via the drinking water at 5 mg/ml. The ^{124}I-iodide PET uptake was measured 1 week after PLX4720 or vehicle treatment, whereas the qPCR and histological analyses were done at the completion of the 2-week study.

Statistics. All statistical analyses were performed using GraphPad Prism version 5.00 for Mac OS X (GraphPad Software). All data are presented as the mean ± SEM. Statistical significance of differences observed between mouse cohorts was determined using 2-tailed unpaired *t* test with a significance criterion of $P < 0.05$. The microPET-derived decay-corrected ^{124}I-iodide time-activity data (%ID/g) for the thyroid/thyroid tumor were fitted to a monoexponential function using the NUMWIN module of the SAAM II computer program, deriving the best-fit uptake (%ID/g at time 0 after injection) and biological half-time (h) for each mouse and the standard deviations of the respective best-fit parameters. The respective *t* statistics for the uptakes and the biological half-times in the 1-week-off and the PLX4720-treated groups of mice were then calculated.

Study approvals. Animal care and all procedures were approved by the Memorial Sloan-Kettering Cancer Center Institutional Animal Care and Use Committee. All studies involving the use of radioactivity were approved by the Memorial Sloan-Kettering Cancer Center Committee on Radiation.

Acknowledgments

This work was supported by NIH grants CA50706, CA72597, DK 15070, and DK20595; the Margot Rosenberg Pulitzer Foundation; and the Lefkofsky Family Foundation. Partial support for the ^{124}I-iodide studies was from the In Vivo Center for Cellular and Molecular Imaging (ICMIC) (P50 086438-10). We also thank Nancy Carrasco for providing the human NIS antibody; Katia Manova, Sho Fujisawa, and Yevgeniy Romin of the Molecular Cytology Core facility; Nancy Pinard and Maria S. Jiao of the Genetically Modified Animal Phenotyping Core; and Regina Feldman and Blesida Punzalan for their invaluable technical support. Technical services provided by the Memorial Sloan-Kettering Cancer Center Small-Animal Imaging Core Facility, supported in part by NIH Small-Animal Imaging Research Program (SAIRP) grant no. R24 CA83084 and NIH Center grant no. P30 CA08748, are gratefully acknowledged.

Received for publication August 11, 2011, and accepted in revised form October 12, 2011.

Address correspondence to: James A. Fagin, Memorial Sloan-Kettering Cancer Center, 1275 York Avenue, Box 296, Zuckerman Bld., ZRC 504, New York, New York 10065, USA. Phone: 646.888.2136; Fax: 646.422.0890; E-mail: faginj@mskcc.org.

1. Davies H, et al. Mutations of the BRAF gene in human cancer. *Nature*. 2002;417(6892):949–954.
2. Kimura ET, Nikiforova MN, Zhu Z, Knauf JA, Nikiforov YE, Fagin JA. High prevalence of BRAF mutations in thyroid cancer: genetic evidence for constitutive activation of the RET/PTC-RAS-BRAF signaling pathway in papillary thyroid carcinoma. *Cancer Res*. 2003;63(7):1454–1457.
3. Nikiforova MN, et al. BRAF mutations in thyroid tumors are restricted to papillary carcinomas and anaplastic or poorly differentiated carcinomas arising from papillary carcinomas. *J Clin Endocrinol Metab*. 2003;88(11):5399–5404.
4. Xing M, et al. BRAF mutation predicts a poorer clinical prognosis for papillary thyroid cancer. *J Clin Endocrinol Metab*. 2005;90(12):6373–6379.
5. Elisei R, et al. BRAF(V600E) mutation and outcome of patients with papillary thyroid carcinoma: a 15-year median follow-up study. *J Clin Endocrinol Metab*. 2008;93(10):3943–3949.
6. Ricarte-Filho JC, et al. Mutational profile of advanced primary and metastatic radioactive iodine-refractory thyroid cancers reveals distinct pathogenetic roles for BRAF, PIK3CA, and AKT1. *Cancer Res*. 2009;69(11):4885–4893.
7. Sedliarou I, et al. The BRAFT1796A transversion is a prevalent mutational event in human thyroid microcarcinoma. *Int J Oncol*. 2004;25(6):1729–1735.
8. Weinstein IB. Cancer. Addiction to oncogenes--the Achilles heal of cancer. *Science*. 2002;297(5578):63–64.
9. Yokoyama K, Imamoto F. Transcriptional control of the endogenous MYC protooncogene by antisense RNA. *Proc Natl Acad Sci U S A*. 1987;84(21):7363–7367.
10. Loke SL, Stein C, Zhang X, Avigan M, Cohen J, Neckers LM. Delivery of c-myc antisense phosphorothioate oligodeoxynucleotides to hematopoietic cells in culture by liposome fusion: specific reduction in c-myc protein expression correlates with

inhibition of cell growth and DNA synthesis. *Curr Top Microbiol Immunol*. 1988;141:282–289.
11. Mukhopadhyay T, Tainsky M, Cavender AC, Roth JA. Specific inhibition of K-ras expression and tumorigenicity of lung cancer cells by antisense RNA. *Cancer Res*. 1991;51(6):1744–1748.
12. Aoki K, Yoshida T, Matsumoto N, Ide H, Sugimura T, Terada M. Suppression of Ki-ras p21 levels leading to growth inhibition of pancreatic cancer cell lines with Ki-ras mutation but not those without Ki-ras mutation. *Mol Carcinog*. 1997;20(2):251–258.
13. Colomer R, Lupu R, Bacus SS, Gelmann EP. erbB-2 antisense oligonucleotides inhibit the proliferation of breast carcinoma cells with erbB-2 oncogene amplification. *Br J Cancer*. 1994;70(5):819–825.
14. Mitsutake N, Knauf JA, Mitsutake S, Mesa C Jr, Zhang L, Fagin JA. Conditional BRAFV600E expression induces DNA synthesis, apoptosis, dedifferentiation, and chromosomal instability in thyroid PCCL3 cells. *Cancer Res*. 2005;65(6):2465–2473.
15. Mesa C Jr, et al. Conditional activation of RET/PTC3 and BRAFV600E in thyroid cells is associated with gene expression profiles that predict a preferential role of BRAF in extracellular matrix remodeling. *Cancer Res*. 2006;66(13):6521–6529.
16. Felsher DW, Bishop JM. Reversible tumorigenesis by MYC in hematopoietic lineages. *Mol Cell*. 1999;4(2):199–207.
17. Chin L, et al. Essential role for oncogenic Ras in tumour maintenance. *Nature*. 1999; 400(6743):468–472.
18. Fisher GH, et al. Induction and apoptotic regression of lung adenocarcinomas by regulation of a K-Ras transgene in the presence and absence of tumor suppressor genes. *Genes Dev*. 2001;15(24):3249–3262.
19. Huettner CS, Zhang P, Van Etten RA, Tenen DG. Reversibility of acute B-cell leukaemia induced by BCR-ABL1. *Nat Genet*. 2000;24(1):57–60.
20. Moody SE, et al. Conditional activation of Neu in the mammary epithelium of transgenic mice results in reversible pulmonary metastasis. *Cancer Cell*. 2002;2(6):451–461.
21. Dhomen N, et al. Oncogenic Braf induces melanocyte senescence and melanoma in mice. *Cancer Cell*. 2009;15(4):294–303.
22. Ball DW, et al. Selective growth inhibition in BRAF mutant thyroid cancer by the mitogen-activated protein kinase kinase 1/2 inhibitor AZD6244. *J Clin Endocrinol Metab*. 2007;92(12):4712–4718.
23. Leboeuf R, et al. BRAFV600E mutation is associated with preferential sensitivity to mitogen-activated protein kinase kinase inhibition in thyroid cancer cell lines. *J Clin Endocrinol Metab*. 2008;93(6):2194–2201.
24. Salerno P, et al. Cytostatic activity of adenosine triphosphate-competitive kinase inhibitors in BRAF mutant thyroid carcinoma cells. *J Clin Endocrinol Metab*. 2010;95(1):450–455.
25. Nucera C, et al. B-Raf(V600E) and thrombospondin-1 promote thyroid cancer progression. *Proc Natl Acad Sci U S A*. 2010;107(23):10649–10654.
26. Solit DB, et al. BRAF mutation predicts sensitivity to MEK inhibition. *Nature*. 2006;439(7074):358–362.
27. Joseph EW, et al. The RAF inhibitor PLX4032 inhibits ERK signaling and tumor cell proliferation in a V600E BRAF-selective manner. *Proc Natl Acad Sci U S A*. 2010;107(33):14903–14908.
28. Tsai J, et al. Discovery of a selective inhibitor of oncogenic B-Raf kinase with potent antimelanoma activity. *Proc Natl Acad Sci U S A*. 2008;105(8):3041–3046.
29. Flaherty KT, et al. Inhibition of mutated, activated BRAF in metastatic melanoma. *N Engl J Med*. 2010; 363(9):809–819.
30. Poulikakos PI, Zhang C, Bollag G, Shokat KM, Rosen N. RAF inhibitors transactivate RAF dimers and ERK signalling in cells with wild-type BRAF. *Nature*. 2010;464(7287):427–430.
31. D'Cruz CM, et al. c-MYC induces mammary tumorigenesis by means of a preferred pathway involving spontaneous Kras2 mutations. *Nat Med*. 2001; 7(2):235–239.
32. Franco AT, et al. Thyrotrophin receptor signaling dependence of Braf-induced thyroid tumor initiation in mice. *Proc Natl Acad Sci U S A*. 2011; 108(4):1615–1620.
33. Charles RP, Iezza G, Amendola E, Dankort D, McMahon M. Mutationally activated BRAF(V600E) elicits papillary thyroid cancer in the adult mouse. *Cancer Res*. 2011;71(11):3863–3871.
34. Jechlinger M, Podsypanina K, Varmus H. Regulation of transgenes in three-dimensional cultures of primary mouse mammary cells demonstrates oncogene dependence and identifies cells that survive deinduction. *Genes Dev*. 2009;23(14):1677–1688.
35. Soares P, et al. BRAF mutations and RET/PTC rearrangements are alternative events in the etiopathogenesis of PTC. *Oncogene*. 2003;22(29):4578–4580.
36. Frattini M, et al. Alternative mutations of BRAF, RET and NTRK1 are associated with similar but distinct gene expression patterns in papillary thyroid cancer. *Oncogene*. 2004;23(44):7436–7440.
37. De Vita G, et al. Expression of the RET/PTC1 oncogene impairs the activity of TTF-1 and Pax-8 thyroid transcription factors. *Cell Growth Differ*. 1998; 9(1):97–103.
38. Portella G, et al. Human N-ras, TRK-T1, and RET/PTC3 oncogenes, driven by a thyroglobulin promoter, differently affect the expression of differentiation markers and the proliferation of thyroid epithelial cells. *Oncol Res*. 1999;11(9):421–427.
39. Knauf JA, Kuroda H, Basu S, Fagin JA. RET/PTC-induced dedifferentiation of thyroid cells is mediated through Y1062 signaling through SHC-RAS-MAP kinase. *Oncogene*. 2003;22(28):4406–4412.
40. Riesco-Eizaguirre G, et al. The BRAFV600E oncogene induces transforming growth factor beta secretion leading to sodium iodide symporter repression and increased malignancy in thyroid cancer. *Cancer Res*. 2009;69(21):8317–8325.
41. Costamagna E, Garcia B, Santisteban P. The functional interaction between the paired domain transcription factor Pax8 and Smad3 is involved in transforming growth factor-beta repression of the sodium/iodide symporter gene. *J Biol Chem*. 2004; 279(5):3439–3446.
42. Bollag G, et al. Clinical efficacy of a RAF inhibitor needs broad target blockade in BRAF-mutant melanoma. *Nature*. 2010;467(7315):596–599.
43. Durante C, et al. BRAF mutations in papillary thyroid carcinomas inhibit genes involved in iodine metabolism. *J Clin Endocrinol Metab*. 2007; 92(7):2840–2843.
44. Muller PY, Janovjak H, Miserez AR, Dobbie Z. Processing of gene expression data generated by quantitative real–time RT–PCR. *Biotechniques*. 2002; 32(6):1372–1374.
45. Pohlenz J, Maqueem A, Cua K, Weiss RE, Van Sande J, Refetoff S. Improved radioimmunoassay for measurement of mouse thyrotropin in serum: strain differences in thyrotropin concentration and thyrotroph sensitivity to thyroid hormone. *Thyroid*. 1999;9(12):1265–1271.
46. Sheh Y, Koziorowski J, Balatoni J, Lom C, Dahl JR, Finn RD. Low energy cyclotron production and chemical separation of "no carrier added" iodine-124 from a reusable, enriched tellurium-124 dioxide/aluminum oxide solid solution target? *Radiochimica Acta*. 2000;88(3–4):169–173.